Progress In Electromagnetics Research M, Vol. 113, 237–247, 2022

A Defected Circular Ring Dual-Band MIMO Antenna with High Isolation for 5G and IEEE 802.11 a/ac/ax

Jing Cai[1], Jianlin Huang[1], Bo Chen[1], Lingrong Shen[1], Tian Hong Loh[2], and Gui Liu[1, *]

Abstract—The design and analysis of a dual-band two-port multiple-input multiple-output (MIMO) antenna with high isolation suitable for fifth-generation (5G) and wireless local area network (WLAN) applications are introduced in this paper. On the top of the substrate, the proposed antenna element is mainly composed of a defected circular ring with an L-shaped strip, an F-shaped stub, and an L-shaped stub. The bottom of the substrate comprises two rectangular defected ground structures and a neutral line with two Y-shaped stubs. The antenna isolation structure is employed to minimize the coupling between antenna elements, which is larger than 15 dB. The overall dimension of the proposed two-port MIMO antenna is approximately 45 mm × 45 mm × 1.59 mm. The measured −10 dB impedance frequency bands include 3.28–3.72 GHz and 4.44–5.92 GHz, which can cover 5G (3.3–3.6 GHz and 4.8–5 GHz) and IEEE 802.11 a/ac/ax (5.15–5.35 GHz and 5.47–5.85 GHz). The measured efficiency is greater than 60% and 55% at the lower and higher frequency bands. The measured peak gain ranges from 4 dBi to 5.8 dBi in both operating frequency bands. The proposed MIMO antenna is feasible for the 5G and WLAN applications.

1. INTRODUCTION

The rapid development of 5G wireless communication antennas has received more and more attention [1–5]. Research on the antennas for 5G base stations and mobile terminals is becoming increasingly important. Multiple-input multiple-output (MIMO) [6, 7] is an effective method to improve channel capacity and has been regarded as one of the critical techniques for 5G mobile communication systems [8, 9]. Exploiting multipath characteristics enables high data capacity [10], transmission speed, and spectral efficiency without increasing the input power [11, 12]. Therefore, developing MIMO antennas is of great importance [13].

However, the mutual coupling between antennas will degrade the performance of MIMO systems. To ameliorate the isolation between multiple antenna elements, various decoupling techniques have been widely investigated, such as self-curing decoupling [14], neutralization lines [15], defected ground structure (DGS) [16–18], decoupling surface [19], self-decoupled [20], and parasitic decoupling elements [21]. The following is a description of some decoupling technologies in detail. In [14], the mutual coupling between antenna elements can be reduced by inlaying lumped element capacitors on the ground plane. A rectangular microstrip stub with a defected ground plane to achieve high isolation of larger than 15 dB between the two antenna elements is presented in [15]. The proposed antenna in [21] consists of parasitic elements and a defective ground plane, which can improve the isolation performance. However, designing a miniaturized antenna with high isolation and low correlation is still challenging.

Received 1 August 2022, Accepted 16 September 2022, Scheduled 10 October 2022
* Corresponding author: Gui Liu (iitgliu2@gmail.com).
[1] College of Electrical and Electronic Engineering, Wenzhou University, Wenzhou 325035, Zhejiang, China. [2] National Physical Laboratory, Teddington TW11 0LW, UK.

This paper develops a miniaturized dual-band two-port MIMO antenna for 5G (3.3–3.6 GHz and 4.8–5 GHz) and IEEE 802.11 a/ac/ax (5.15–5.35 GHz and 5.47–5.85 GHz) applications. The proposed MIMO antenna shows high isolation, high gain, and low envelope correlation coefficient (ECC), which can be used to realize high transmission rates, large channel capacity, and spectral efficiency. The radiator of each MIMO antenna element is formed of a defected circular ring with an L-shaped strip, an F-shaped stub, and an L-shaped stub. A T-shaped neutral line with two Y-shaped stubs is employed to enhance the isolation between two antenna elements and achieve low correlation.

2. DESIGN OF THE PROPOSED MIMO ANTENNA

The geometry of the developed antenna is presented in Figure 1. The proposed MIMO antenna is fabricated on an FR-4 substrate with a thickness of 1.59 mm, relative permittivity εr of 4.4, and loss $\tan\delta$ of 0.02. Two identical radiating elements fed through 3 mm-wide microstrip lines are put vertically on the top side of the substrate. The antenna element consists of a defected circular ring with an L-shaped strip, an F-shaped stub, and an L-shaped stub. On the bottom side of the introduced antenna, there is an isolation structure made up of a T-shaped neutral line and two Y-shaped stubs. The dimensions of the optimized antenna are listed in Table 1.

In Figure 2, the evolution of the presented antenna structure and simulated S_{11} are shown. The

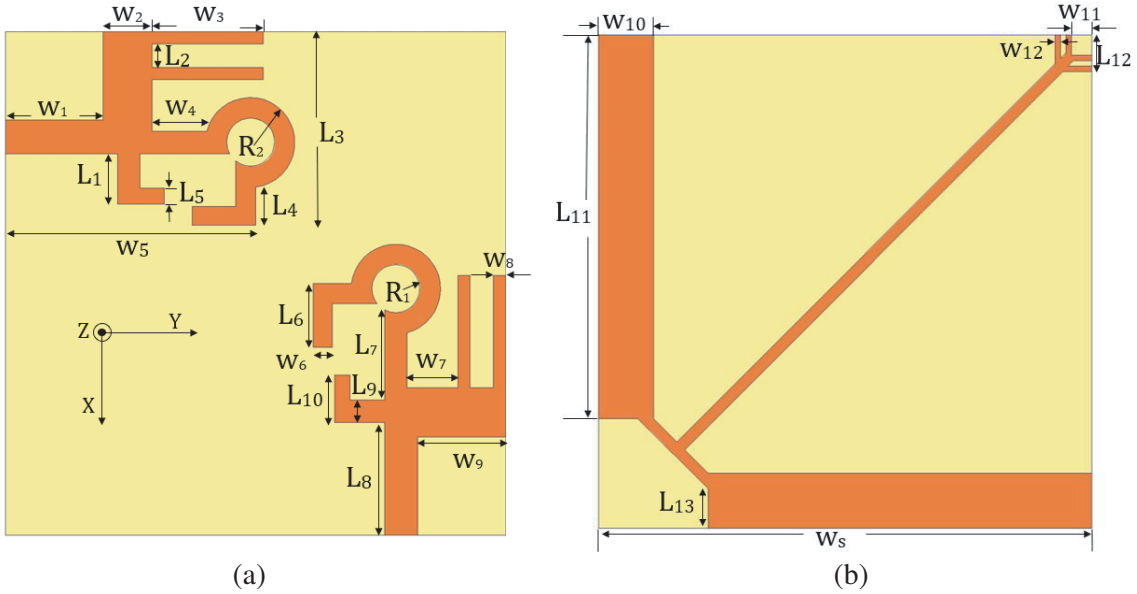

Figure 1. The geometry of the developed MIMO antenna. (a) Top view. (b) Bottom view.

Table 1. Parameters of the proposed antenna (in millimeters).

Parameter	W_1	W_2	W_3	W_4	W_5	W_6	W_7
Value	8.8	4.4	10.0	4.9	22.5	1.7	4.6
Parameter	W_8	W_9	W_{10}	W_{11}	W_{12}	W_s	L_1
Value	1.1	7.9	5.0	1.8	0.5	45	4.5
Parameter	L_2	L_3	L_4	L_5	L_6	L_7	L_8
Value	2.1	17.3	3.4	1.4	5.7	8.0	10.1
Parameter	L_9	L_{10}	L_{11}	L_{12}	L_{13}	R_1	R_2
Value	2.0	4.2	35.0	3.3	3.6	2.15	4.25

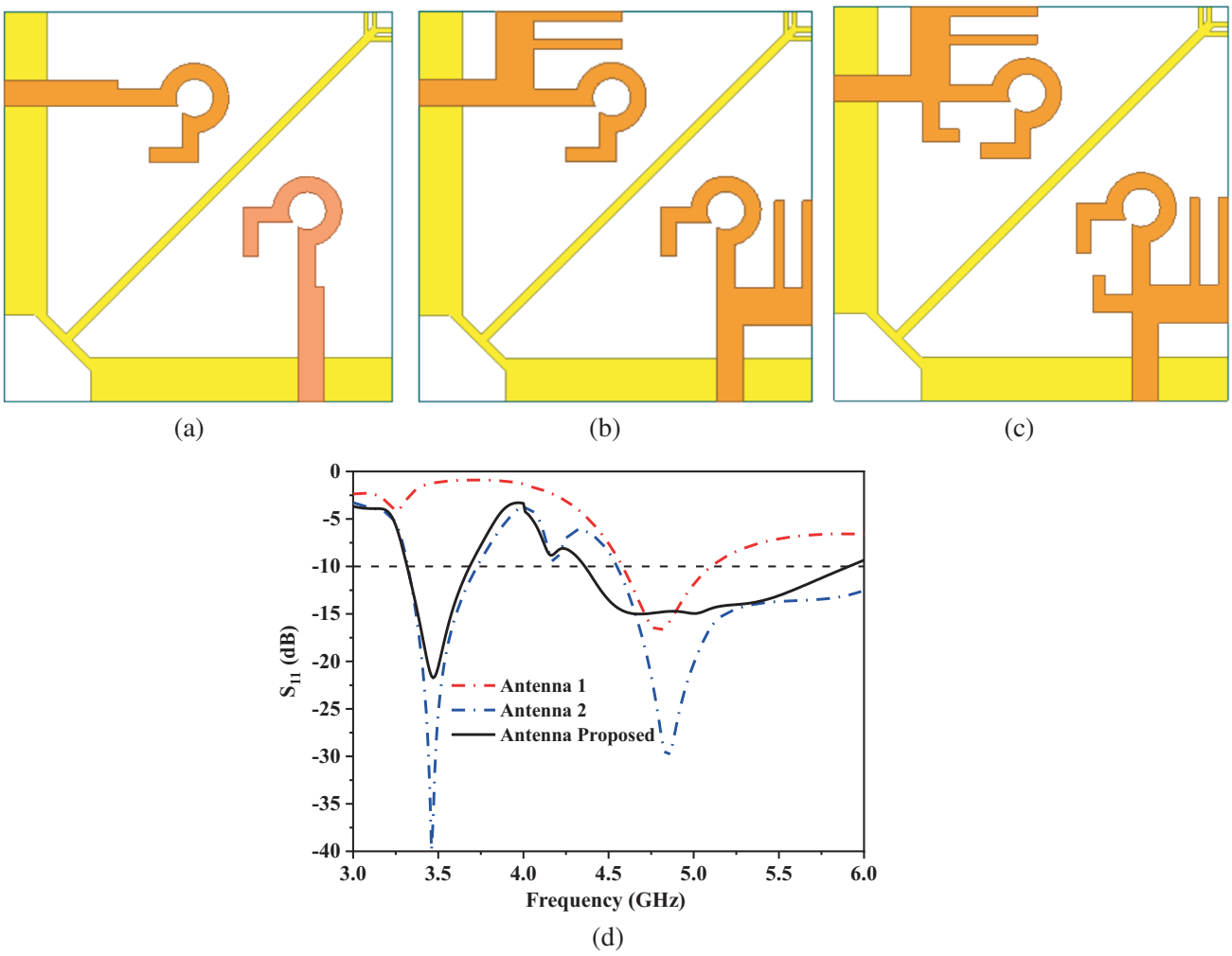

Figure 2. Evolution of the proposed antenna. (a) Structure of antenna 1. (b) Structure of antenna 2. (c) Structure of the proposed antenna. (d) Simulated S_{11}.

introduction of the F-shaped stub in antenna 2 can be used to tune the S_{11} of antenna 1 to be smaller than -10 dB in two operating frequency bands. The introduction of the L-shaped stub in the proposed antenna can be used to tune S_{11} of antenna 2 to the lower frequencies in the higher frequency band, while those in the lower frequency band remain almost unchanged.

3. SIMULATED RESULTS AND ANALYSIS

In order to find out the key parameters affecting the performance of the proposed MIMO antenna, the simulated surface current distributions are illustrated in Figure 3. As shown in Figure 3, the upper half of the F-shaped stub, the defected circular ring, and the L-shaped strip mostly realize the impedance matching of the desired frequency bands. When the antenna operates at 3.5 GHz, the current distributions mainly occur on the upper half of the F-shaped stub, as shown in Figure 3(a). The current concentrates at part of the defected circular ring and the L-shaped strip at 5 GHz, as illustrated in Figure 3(b). Hence, the size of the F-shaped stub and T-shaped strip can be adjusted to optimize the resonance frequencies and isolation.

In Figure 4, W_3 and L_5 can be used to tune the resonance frequencies. Figure 4(a) shows the simulated reflection coefficients of the proposed antenna with different values of W_3. It suggests that

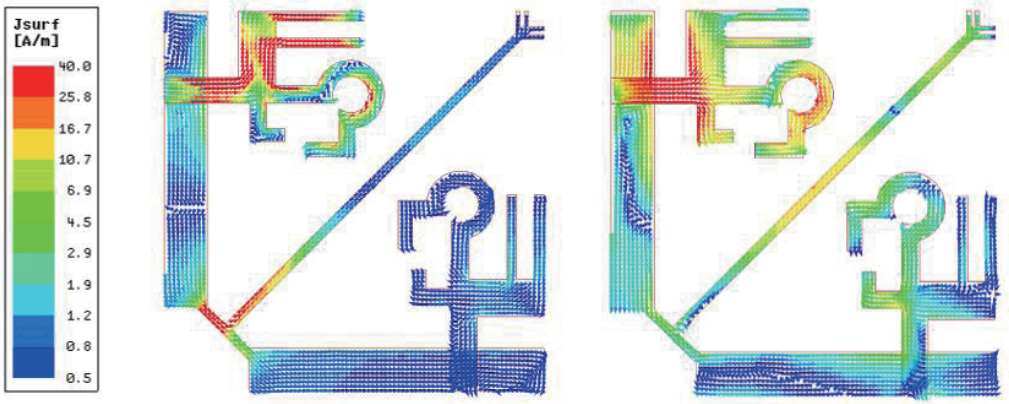

Figure 3. Simulated surface current distribution at two resonant frequencies. (a) 3.5 GHz. (b) 5 GHz.

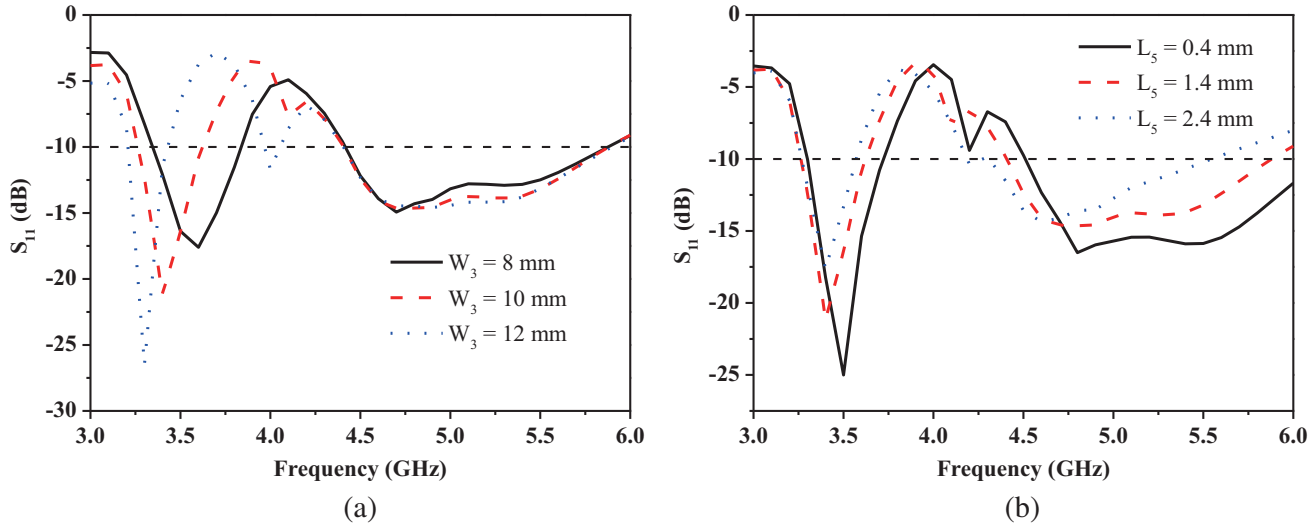

Figure 4. Simulated reflection coefficients of the proposed antenna with two different values. (a) W_3. (b) L_5.

W_3 has a strong impact on the lower frequency band but less on the higher frequency band. When the value of W_3 is 10 mm, the −10 dB impedance bandwidth of the lower frequency is 330 MHz (3.29 to 3.62 GHz), which covers the frequency band of 3.3–3.6 GHz. As illustrated in Figure 4(b), the value of L_5 affects the higher frequency band while the lower frequency band remains almost unchanged. The simulation results suggest that the optimized value of L_5 is 1.4 mm, and the −10 dB impedance bandwidth of the higher frequency is 1470 MHz (4.41 to 5.88 GHz), which covers both 5.15–5.35 GHz and 5.47–5.85 GHz frequency bands.

The isolation between two antenna elements can be improved by implementing an isolation structure consisting of a T-shaped neutral line and two Y-shaped stubs. The T-shaped neutral line acts as a band-stop filter to minimize surface currents, and the two Y-shaped stubs are introduced to improve bandwidth. In Figure 5, the simulated isolation of the proposed antenna with/without the isolation structure is presented. It indicates that the proposed structure can effectively increase the isolation at the lower frequency band.

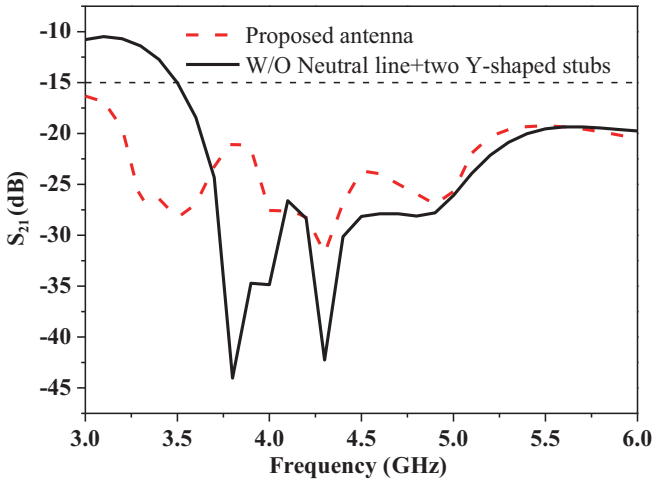

Figure 5. Simulated isolation of the developed antenna with/without isolation structure.

(a) (b)

Figure 6. Photograph of the fabricated antenna. (a) Top view. (b) Bottom view.

4. MEASURED RESULTS AND DISCUSSION

Figure 6 shows the photographs of the fabricated antenna. The simulated and measured reflection coefficients are shown in Figure 7. There is a small amount of error between the measurement and simulation results, which is due to several different reasons, such as the fabrication tolerance and loss tangent of the substrate material. From the measurement results, it can be seen that the measured -10 dB reflection coefficients are 440 MHz (3.28–3.72 GHz) and 1480 MHz (4.44–5.92 GHz), which can cover 5G (3.3–3.6 GHz and 4.8–5 GHz) and IEEE 802.11 a/ac/ax (5.15–5.35 GHz and 5.47–5.85 GHz) frequency bands.

Figure 8 depicts the simulated and measured isolation in the frequency band of 3–6 GHz, which contains four frequency bands (3.3–3.6 GHz, 4.8–5 GHz, 5.15–5.35 GHz, and 5.47–5.85 GHz). The measured S_{21} is less than -15 dB in the desired frequency bands. The measured isolation between two ports agrees well with the simulated results. The slight frequency deviation is mainly due to SMA connective errors.

The measured and simulated radiation patterns at 3.5 GHz and 5 GHz of the proposed antenna are illustrated in Figure 9. For the measurement results, the co-pol is in the black solid line and the cross-pol in the green dotted line, and for the simulation results, the co-pol is in the red solid line and the cross-pol in the blue dotted line. The E-plane represents the flow direction of the feed current, and

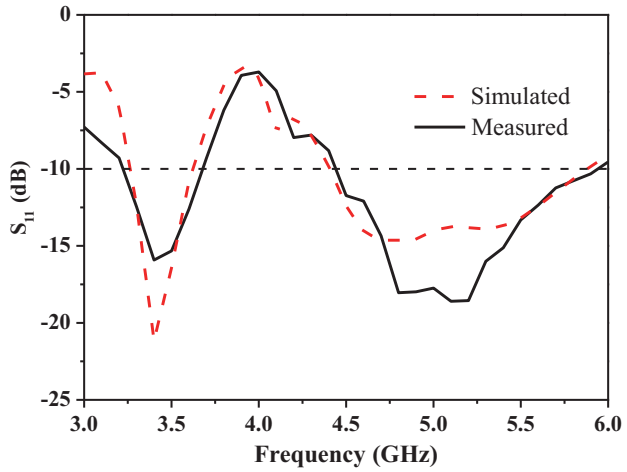

Figure 7. Simulated and measured reflection coefficients of the proposed antenna.

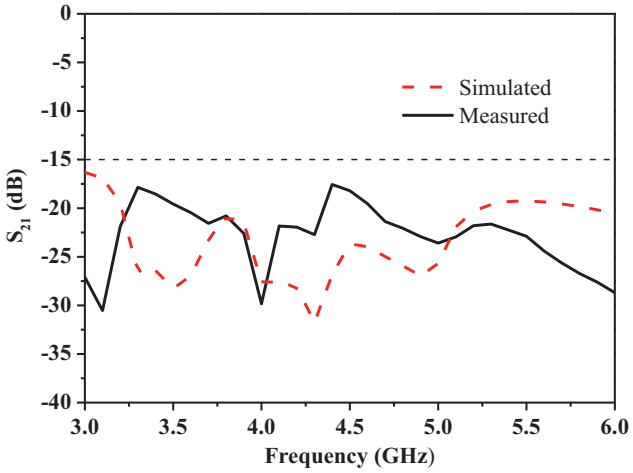

Figure 8. Simulated and measured isolation of the proposed antenna.

H-plane is perpendicular to that direction.

As shown in Figure 10, the measured and simulated peak gains and efficiencies are demonstrated. The measurement results show that the proposed antenna's efficiency is greater than 60% and 55% at both operating frequency bands. The gain of the designed antenna ranges from 4 dBi to 5.8 dBi at both operating frequency bands.

The ECC is a crucial parameter to illustrate the correlation between communication channels. If taking the proposed dual-band MIMO antenna as an example, its ECC value can be expressed as Equation (1) [19]:

$$\rho_e = \frac{\left|S_{11}^* S'_{12} + S_{21}^* S'_{22}\right|^2}{\left(1 - \left(|S_{11}|^2 + |S_{21}|^2\right)\right)\left(1 - \left(|S_{22}|^2 + |S_{12}|^2\right)\right)} \tag{1}$$

where S_{11}^* and S_{21}^* are the imaginary parts of S_{11} and S_{21} parameters, respectively. S'_{12} and S'_{22} are the real parts of the S_{12} and S_{22} parameters, respectively.

In Figure 11, the calculated ECC results of the proposed MIMO antenna are presented. It demonstrates that the calculated ECC is very low over the desired frequency bands, and the maximum value is 0.003.

The calculated diversity gain (DG) is related to ECC in Equation (2) [14]:

$$\mathrm{DG} = 10 \times \sqrt{1 - |ECC|^2} \tag{2}$$

In Figure 12, the calculated DG of the proposed dual-band MIMO antenna is presented. It can be seen that the values of DG in the desired frequency bands are greater than 9.98.

The multiplexing efficiency (ME) is related to ECC in Equation (3) [3]. η_1 and η_2 are efficiencies in Figure 10.

$$\mathrm{ME} = \sqrt{\eta_1 \eta_2 \left(1 - |ECC|^2\right)} \tag{3}$$

The calculated ME of the proposed antenna is shown in Figure 13. The values of ME in the operating frequency bands are greater than 60%.

The total active reflection coefficient (TARC) is an essential index for reflecting the performance of the MIMO antenna, which can be used to judge the influence on impedance bandwidth when adjacent antennas work at the same time. The TARC parameters of the fabricated antenna can be obtained by Equation (4) [3]:

$$\mathrm{TARC} = \sqrt{\frac{(S_{11} + S_{12})^2 + (S_{21} + S_{22})^2}{2}} \tag{4}$$

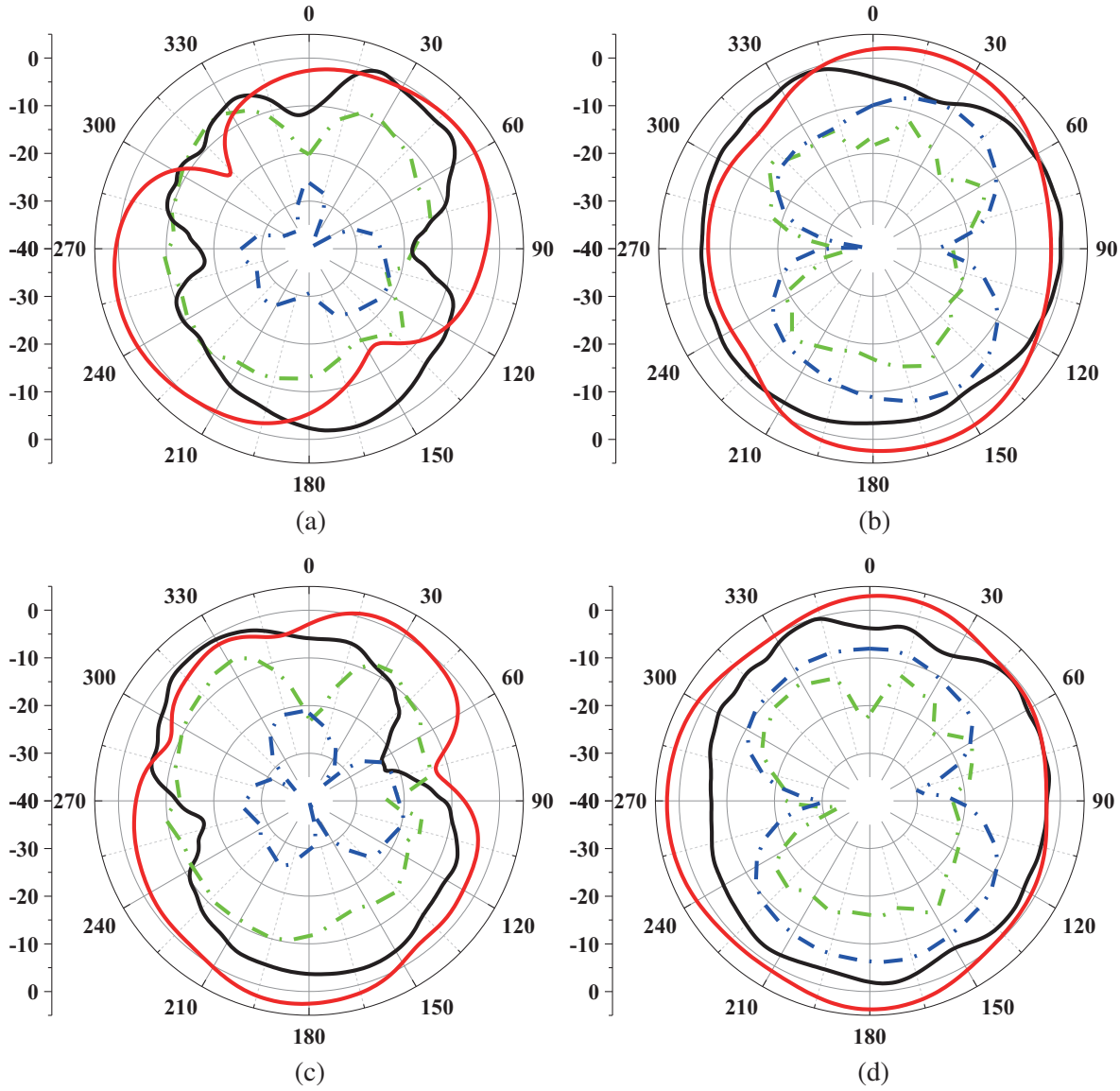

Figure 9. Radiating patterns of the proposed antenna. (a) 3.5 GHz E-plane. (b) 3.5 GHz H-plane. (c) 5 GHz E-plane. (d) 5 GHz H-plane.

The calculated TARC values are presented in Figure 14. It is observed that the values of TARC in the operating frequency bands are lower than -10 dB, which proves that the MIMO system is stable.

For MIMO antenna systems, the upper limit of the information transmission rate in the wireless communication channel can be determined by channel capacity loss (CCL), and CCL can be expressed as Equation (5) [4]:

$$\mathrm{CCL}\,(\mathrm{loss}) = -\log_2\left[\det\left(\psi^R\right)\right] \tag{5}$$

where ψ^R is the element matrix calculated from S-parameter and can be expressed as Equation (6) [4]:

$$\left(\psi^R\right) = \begin{bmatrix} \rho_{11} & \rho_{12} \\ \rho_{21} & \rho_{22} \end{bmatrix} \tag{6}$$

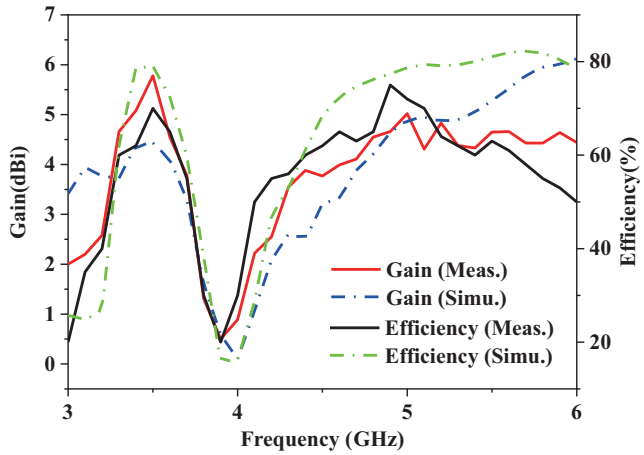

Figure 10. Measured peak gain and efficiency of the proposed antenna.

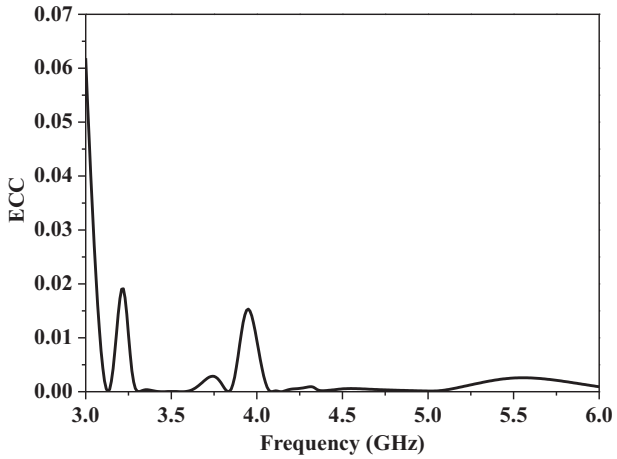

Figure 11. Calculated ECC of the proposed antenna.

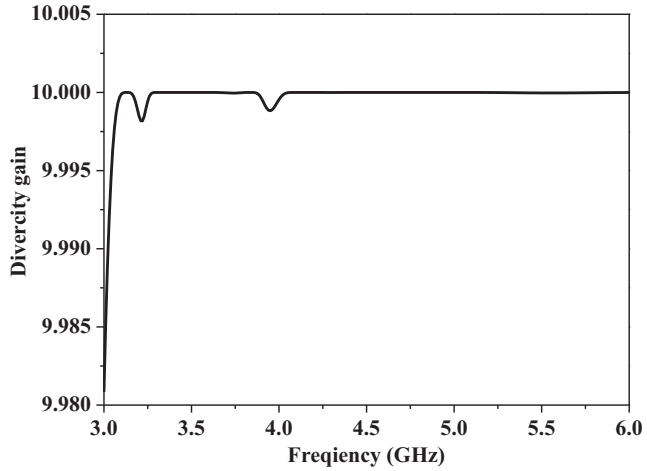

Figure 12. Calculated DG of the proposed antenna.

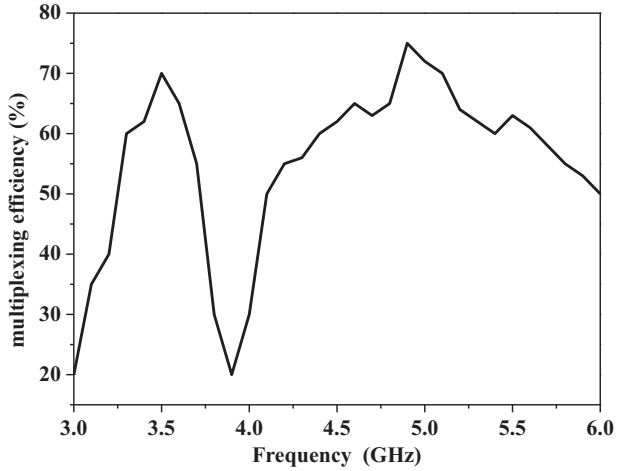

Figure 13. Calculated ME of the proposed antenna.

Matrix elements can be obtained through S-parameters as Equation (7) and Equation (8) [11]:

$$\rho_{ii} = 1 - \left(\sum_{n=1}^{N} |S_{in}^{*} S_{ni}| \right) = 1 - \left(|S_{ii}|^2 + |S_{ij}|^2 \right) \tag{7}$$

$$\rho_{ij} = - \left[\sum_{n=1}^{N} |S_{in}^{*} S_{nj}| \right] = - \left(S_{ii}^{*} S_{ij} + S_{ji}^{*} S_{jj} \right) \tag{8}$$

where $i, j = 1$ or 2, and $n = 1, 2$. The measured result of CCL is depicted in Figure 14. It can be seen that CCL values at 3.5 GHz and 5 GHz are 0.005 bpc/Hz and 0.1 bpc/Hz, respectively. The CCL values of both frequency bands are far below the required 0.5 bpc/Hz.

In Table 2, a comparison of the performances of the designed MIMO antenna with other published antennas is presented. According to the results, the bandwidth of the proposed antenna is wider than that of the antennas demonstrated in [7, 17]. The efficiency of the proposed antenna is higher than that of the antenna presented in [10], and the ECC values of the designed antenna are lower than those of the antennas shown in [4, 7, 10, 13, 17]. In addition, the size of the proposed antenna is more compact, and the peak gain of the proposed antenna is higher than other referenced antennas.

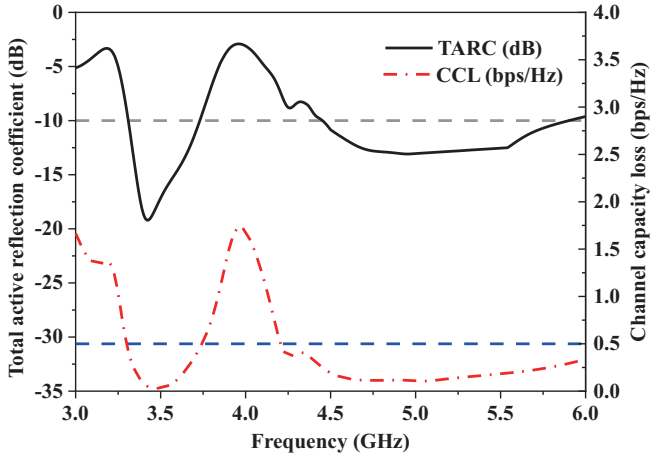

Figure 14. Calculated TARC and CCL of the proposed antenna.

Table 2. Comparison of the designed antenna with other referenced works.

Reference	Operating band (GHz)	Isolation (dB)	Peak Gain (dB)	Efficiency (%)	ECC	Size (mm^3)
[4]	2.42–3.07 4.14–6.37	> 34 > 26	2.8 4.91	74 75	< 0.005	$60 \times 60 \times 1.6$
[7]	3.4–3.8 5.15–5.925	> 12	3	41–82 47–79	< 0.15 < 0.1	$150 \times 80 \times 0.8$
[10]	3.3–3.8 4.8–5.0 5.15–5.925	> 10.5	-	55–72 50–65 43–73	< 0.12	$150 \times 75 \times 0.8$
[13]	2.44–2.47 3.44–3.50 5.15–5.48	> 17 > 18 > 32	5.49 4.57 0.80	-	< 0.03 < 0.035 < 0.005	$54 \times 22 \times 1.6$
[17]	3.4–3.6 4.8–5.0	> 16.5	4.7 5	85 82	< 0.01	$150 \times 75 \times 6.2$
[18]	3.4–3.6 4–8	> 15	3.25 3.40	> 75.1 > 74.2	< 0.003	$21 \times 46 \times 1.6$
This work	3.28–3.72 4.44–5.92	> 15	5.8 5	> 60 > 55	< 0.003	$45 \times 45 \times 1.59$

5. CONCLUSION

A compact dual-band MIMO antenna is introduced in this paper. The radiator of each antenna element is composed of a defected circular ring with an L-shaped strip, an F-shaped stub, and an L-shaped stub. In addition, there are two rectangular defected ground structures and a T-shaped neutral line with two Y-shaped stubs on the bottom of the substrate. The presented antenna operates in the frequency bands of 5G (3.3–3.6 GHz and 4.8–5 GHz) and IEEE 802.11 a/ac/ax (5.15–5.35 GHz and 5.47–5.85 GHz). The measured isolation is lower than -15 dB. The ECC calculated from the experimental S-parameters is lower than 0.005 within both operating bands, which implies excellent diversity for 5G MIMO operation.

ACKNOWLEDGMENT

This work was funded in part by the National Natural Science Foundation of China under Grant No. 61671330, the Science and Technology Department of Zhejiang Province under Grant No. LGG19F010009, and Wenzhou Municipal Science and Technology Program under Grant No. C20170005 and No.2018ZG019.

REFERENCES

1. Morsy, M., "4-port planar MIMO antenna using open-slot radiators for 5G New Radio (NR) frequency bands n38 (2570 to 2620 MHz) and n41 (2496 MHz–2690 MHz) applications," *Progress In Electromagnetics Research Letters*, Vol. 104, 87–94, 2022.
2. Sun, L. B., Y. Li, Z. J. Zhang, and Z. H. Feng, "Wideband 5G MIMO antenna with integrated orthogonal-mode dual-antenna pairs for metal-rimmed smartphones," *IEEE Antennas and Wireless Propagation Letters*, Vol. 68, No. 4, 2494–2503, 2020.
3. Huang, J. L., Z. N. Chen, Q. B. Cai, T. H. Loh, and G. Liu, "Minimized triple-band eight-element antenna array for 5G metal-frame smartphone applications," *Micromachines*, Vol. 13, No. 1, 136–146, 2022.
4. Abhilash, A. P., P. Thomas, K. K. Indhu, K. Neema, R. A. Kumar, and C. Aanandan, "Four-element compact and dual-band MIMO antenna with self-decoupled mechanism for 5G applications," *Progress In Electromagnetics Research C*, Vol. 123, 91–99, 2022.
5. Kumar, D. R. and G. V. Babu, "Six-port quarter wavelength slotted MIMO antenna for 5G mobile phone," *Wireless Personal Communications*, Vol. 120, No. 3, 2043–2059, 2021.
6. Dou, Y. Q., Z. N. Chen, J. Bai, Q. B. Cai, and G. Liu, "Two-port CPW-fed dual-band MIMO antenna for IEEE 802.11 a/b/g applications," *International Journal of Antennas and Propagation*, Vol. 2021, 5572887–5572894, 2021.
7. Li, Y. X., C. Y. D. Sim, Y. Luo, and G. L. Yang, "12-port 5G massive MIMO antenna array in sub-6 GHz mobile handset for LTE bands 42/43/46 applications," *IEEE Access*, Vol. 6, 344–354, 2018.
8. Alhaqbani, H. S., M. M. Bait-Suwailam, M. A. Aldhaeebi, and T. S. Almoneef, "Wideband diversity MIMO antenna design with hexagonal slots for 5G smart mobile terminals," *Progress In Electromagnetics Research C*, Vol. 120, 105–117, 2022.
9. Wei, C. N., Z. Y. Zhang, and K. L. Wu, "Phase compensation for decoupling of large-scale staggered dual-polarized dipole array antennas," *IEEE Antennas and Wireless Propagation Letters*, Vol. 68, No. 4, 2822–2831, 2020.
10. Wang, H. W., R. H. Zhang, Y. Luo, and G. L. Yang, "Compact eight-element antenna array for triple-band MIMO operation in 5G mobile terminals," *IEEE Access*, Vol. 8, 19433–29449, 2020.
11. Dai, X. W., G. Q. Luo, X. H. Zhang, B. You, and H. Y. Jin, "Horizontally polarized wideband antenna based on quarter-wavelength slot elements," *AEU — International Journal of Electronics and Communications*, Vol. 98, 213–219, 2019.
12. Xue, C. D., X. Y. Zhang, Y. F. Cao, Z. J. Hou, and C. F. Ding, "MIMO antenna using hybrid electric and magnetic coupling for isolation enhancement," *IEEE Antennas and Wireless Propagation Letters*, Vol. 65, No. 10, 5162–5170, 2017.
13. Ameen, M., O. Ahmad, and R. K. Chaudhary, "Bandwidth and gain enhancement of triple-band MIMO antenna incorporating metasurface-based reflector for WLAN/WiMAX applications," *IET Microwaves, Antennas & Propagation*, Vol. 14, 1493–1503, 2020.
14. Sui, J. W., Y. H. Dou, X. D. Mei, and K. L. Wu, "Self-curing decoupling technique for MIMO antenna arrays in mobile terminals," *IEEE Antennas and Wireless Propagation Letters*, Vol. 68, No. 2, 838–849, 2020.
15. Yang, R., S. Q. Xi, Q. B. Cai, Z. N. Chen, X. H. Wang, and G. Liu, "A compact planar dual-band multiple-input and multiple-output antenna with high isolation for 5G and 4G applications," *Micromachines*, Vol. 12, No. 5, 544–556, 2021.

16. Pasumarthi, S. R., J. Babu, and A. M. Prasad, "Design of dual band MIMO antenna with improved isolation," *Microwave and Optical Technology Letters*, Vol. 61, No. 6, 1579–1583, 2019.
17. Huang, J. L., G. T. Dong, J. Cai, H. Li, and G. Liu, "A quad-port dual-band MIMO antenna array for 5G smartphone applications," *Electronics*, Vol. 10, No. 5, 542–552, 2021.
18. Ameen, M., O. Ahmad, and R. K. Chaudhary, "Single split-ring resonator loaded self-decoupled dual-polarized MIMO antenna for mid-band 5G and C-band applications," *AEU — International Journal of Electronics and Communications*, Vol. 124, 153336–153348, 2020.
19. Sun, L. B., Y. Li, Z. J. Zhang, and H. Y. Wang, "Self-decoupled MIMO antenna pair with shared radiator for 5G smartphones," *IEEE Antennas and Wireless Propagation Letters*, Vol. 68, No. 5, 3423–3432, 2020.
20. Ren, Z. Y., A. P. Zhao, and S. J. Wu, "MIMO antenna with compact decoupled antenna pairs for 5G mobile terminals," *IEEE Antennas and Wireless Propagation Letters*, Vol. 18, No. 7, 1367–1371, 2019.
21. Peng, H., R. X. Zhi, Q. C. Yang, J. Cai, Y. Wan, and G. Liu, "Design of a MIMO antenna with high gain and enhanced isolation for WLAN applications," *Electronics*, Vol. 10, No. 14, 1659–1669, 2021.